HANSER

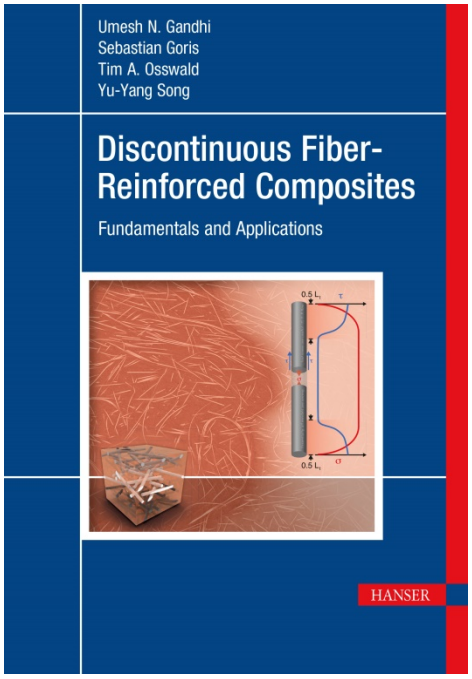

Sample Pages

Discontinuous Fiber-Reinforced Composites

Umesh N. Gandhi et al.

ISBN (Book): 978-1-56990-694-1
ISBN (E-Book): 978-1-56990-695-8

For further information and order see

www.hanserpublications.com (in the Americas)

www.hanser-fachbuch.de (outside the Americas)

Preface

This book is written at an intermediate to advanced level to provide a background on discontinuous fiber-reinforced composites to practicing engineers as well as graduate students. The technical information and practical examples enable the reader to understand the underlying physics and the complex behavior of this unique fiber composite material. Discontinuous fiber-reinforced polymer composites are a growing class of composite materials that are appealing to the aerospace and automotive industries because they are easy to process into components and structures of complex shapes in an automated fashion, using traditional molding techniques or extrusion processes. Compared to the processing of continuous fibers, the automated processes such as injection or compression molding used for discontinuous fibers are quite low cost and suitable for high production rates, which makes them attractive for automobiles and other consumer goods.

Designing with such discontinuous fiber composite material can be quite challenging because the molding process strongly affects the final state of the fibers in the manufactured part. The fiber orientation, fiber length, and fiber concentration can show a large degree of heterogeneity throughout the molded part, especially for complex shaped structures. These variations of the fiber microstructure have a profound impact on the performance of the finished product, evident in the heterogeneous and anisotropic structural properties. This is a challenging situation when compared to isotropic metal parts or continuous fiber-reinforced composites, where the fiber orientation and fiber length are known and are uniform throughout the part. The goal in this book is to provide a theoretical and practical background to address these challenges and provide know-how that will help design parts that are made with discontinuous fiber-reinforced composites, in order to fully exploit the potential of this class of composites.

In the first part of this book the various aspects that lead to the anisotropic properties of the finished parts are covered. Fundamentals of polymeric materials and fibers are discussed, followed by a survey of manufacturing processes used in the industry. The microstructure of fiber-reinforced polymers, with attention to discontinuous fibers, is presented, and fundamental relations between the microstructure and mechanics of fiber-reinforced polymers are developed. The second part of the book explains how the mechanics of fiber-reinforced composites at the micro level can be translated to structural analysis programs, usually at millimeter scale, using a multiscale modeling approach. Furthermore, the fundamentals of mold-filling simulation for injection and compression molding for short and long fibers are included. The third part of the book introduces the reader to practical

examples covering compression molding, injection molding, hybrid structures, and joining. The case studies of practical examples take the readers through all the steps necessary to arrive at a full structural model of a component and compare the predictive models to actual measurements.

Some of the work presented here started in 2012 when the Toyota Research Institute North America (TRINA) began to develop know-how to design lightweight components for automotive applications using discontinuous fiber-reinforced composites. Realizing many fundamental technical challenges, TRINA approached Professor Tim Osswald from the Polymer Engineering Center (PEC) at the University of Wisconsin-Madison for help. What followed was an outstanding collaboration between industry and academia, resulting in significant improvements in the know-how to design using discontinuous fiber-reinforced composites, which is the essence of this book.

The authors would like to acknowledge the invaluable help of many during the preparation of this manuscript. We would like to thank Dr. Huan-Chang Tseng, Dr. Jim Hsu, and Dr. Anthony Yang of CoreTech System for contributing the chapter on process simulation (Chapter 7) and other members of the CoreTech team for their continuous support in many other areas. We are grateful to Tobias Mattner for his outstanding job in not only drawing the figures, but also making excellent suggestions on how to present the information more clearly. We would like to offer special thanks to Prof. Noboru Kikuchi, president of Toyota Central R & D Lab, for the unceasing encouragement to write this book. Takeshi Sekito, Hidetoshi Okada, Masaya Miura, and Yoshinori Suga of Toyota Motor Company for serving as sounding boards and for their technical input. Prof. Uday Vaidya and his group at the University of Tennessee are thanked for their help with the processing technology. We are grateful to Dr. Vlastimil Kunk, from Oakridge National Laboratory, for the help in the characterization of compression molded parts. Dr. Suresh Shah of the Society of Plastics Engineers is thanked for sharing many practical insights and suggestions, and Dr. Danil Prokhorov from TRINA for his continuous cheering and support. Dr. Roger Assaker and his team at e-Xstream Engineering are thanked for their valuable assistance with multiscale modeling. Thanks are due to Dr. Mark Smith and Dr. Julia Diaz Luque of Carl Hanser Verlag for their valuable expertise in editing this book, as well as Jörg Strohbach for his support throughout this project. Above all, the authors would like to thank their families for their continued support of their work and their input throughout the writing of this book.

Umesh N. Gandhi and *Yu-Yang Song* January 2020
Ann Arbor, Michigan, USA

Tim A. Osswald
Madison, Wisconsin, USA

Sebastian Goris
St. Paul, Minnesota, USA

About the Authors

Dr. Umesh N. Gandhi

Umesh Gandhi is Executive Scientist at the Toyota Research Institute North America (TRINA) in Ann Arbor, MI, and was formerly Staff Engineer at General Motors. He holds a Ph.D. from the University of Michigan. His research interests are lightweight and programmable mechanical systems. He has authored more than 50 publications and holds over 40 issued patents.

Prof. Prof. hon. Dr. Tim A. Osswald

Tim Osswald teaches at the University of Wisconsin-Madison and is co-Director of the Polymer Engineering Center. He also holds honorary professorships at the Friedrich Alexander Universität in Erlangen, Germany and the Universidad Nacional de Colombia. He teaches and does research in polymer engineering, a field where he has published 11 books and over 300 papers.

Dr. Sebastian Goris

Sebastian Goris is Sr. Research Engineer at the Corporate Research Process Laboratory at 3M in St. Paul, MN, where he focuses on new technology development in the area of automotive electrification. He received his Ph. D. in Mechanical Engineering at the University of Wisconsin-Madison under Prof. Tim Osswald.

Dr. Yu-Yang Song

Yu-Yang Song is Senior Scientist at the Toyota Research Institute North America (TRINA) in Ann Arbor, MI. His research focuses on lightweight composite materials and textile fabric materials for future mobility applications. He received his Ph. D. in the area of defects detection of aerospace composite at Wayne State University in Detroit, MI.

Contents

Preface V

About the Authors IX

1 Introduction 1

1.1 Historical Background 1

1.2 Fiber-Reinforced Composites 7

1.3 Lightweighting in Automotive Applications 12

1.4 Background and Challenges in Designing with Discontinuous Fibers 20

1.5 Structure and Objectives of this Book 23

References 26

2 Materials 29

2.1 Reinforcing Phase 29

2.1.1 Particle-Reinforced Composites 30

2.1.2 Continuous Fibers 31

2.1.2.1 Woven Fabrics 31

2.1.2.2 Braiding 33

2.1.3 Discontinuous Fibers 34

2.1.4 Sizing 36

2.2 Matrix 37

2.2.1 Thermoplastics 37

2.2.1.1 Amorphous Thermoplastics 43

2.2.1.2 Semi-crystalline Thermoplastics 45

2.2.2 Thermosets 47

2.2.2.1 Curing Reaction 50

References 57

3 Manufacturing Processes ... 59

3.1 Fiber-Reinforced Thermoset Molding Processes ... 59
3.1.1 Compression Molding of Sheet Molding Compound ... 60
3.1.2 Injection-Compression Molding of Bulk Molding Compound ... 64

3.2 Fiber-Reinforced Thermoplastics ... 65
3.2.1 Injection Molding ... 66
3.2.2 Extrusion Compression Molding ... 76
3.2.3 GMT Compression Molding ... 78

3.3 Additive Manufacturing ... 80

3.4 Vacuum Bagging Techniques ... 83
3.4.1 Fiber Spray-up Molding ... 83
3.4.2 Hand-Layup Molding ... 84
3.4.3 Vacuum-Assisted Resin Infusion ... 85
3.4.4 Resin Transfer Molding Techniques ... 88

3.5 Processes Involving Hybrid Structures ... 93

References ... 94

4 Microstructure in Discontinuous Fiber-Reinforced Composites ... 95

4.1 Process-Induced Microstructure in Discontinuous Fiber-Reinforced Composites ... 95
4.1.1 Fiber Attrition ... 96
4.1.2 Fiber Alignment ... 101
4.1.3 Fiber–Matrix Separation ... 106
4.1.4 Fiber–Matrix Bonding ... 110
4.1.5 Microstructure–Property Relationship ... 111

4.2 Characterization Techniques for Fiber Microstructure Analysis ... 115
4.2.1 Measuring Fiber Orientation ... 116
4.2.2 Review of Fiber Length Measurement Methods ... 129
4.2.2.1 Comparative Study of Measurement Techniques ... 139
4.2.3 Measuring Fiber Concentration ... 145
4.2.4 Fiber Microstructure Characterization Conclusions ... 151

4.3 Case Study: LFT Injection Molding of a Simple Plaque Geometry ... 153
4.3.1 Analysis of the Process-Induced Fiber Alignment ... 156
4.3.2 Analysis of the Process-Induced Fiber Breakage ... 158
4.3.3 Analysis of the Process-Induced Fiber Concentration ... 160
4.3.3.1 Flow Front Analysis ... 163
4.3.4 Discussion and Conclusions ... 166

References ... 172

5 Mechanics of Composites **177**
Paul V. Osswald and Tim A. Osswald

5.1 Anisotropic Strain–Stress Relation 178

5.2 Laminated Composite 179
5.2.1 Equilibrium, Deformation, and Constitutive Equations 180
5.2.2 Transverse Properties—The Halpin-Tsai Equation 181
5.2.3 Transformation of Fiber-Reinforced Composite Laminate Properties 184
5.2.4 Sample Application of a Laminated Composite 187

5.3 Discontinuous Fiber-Reinforced Composites 190
5.3.1 Sample Application of Critical Length for Load Transfer 193
5.3.2 Reinforced Composite Laminates with a Fiber Orientation Distribution Function 197

5.4 Failure of Fiber-Reinforced Composites 198
5.4.1 Failure of an Axially Loaded Laminate 198

5.5 Failure Criteria for Composites with Complex Loads 200
5.5.1 Maximum Stress Failure Criterion 201
5.5.2 Tsai-Hill Failure Criterion 203
5.5.3 A New Strength Tensor Based Failure Criterion with Stress Interactions 205

References 215

6 Modeling and Simulation of Discontinuous Fiber-Reinforced Composites **217**

6.1 Introduction to Finite Element Methods (FEM) 217
6.1.1 Basic Concept of FEM 218
6.1.2 Status of FEM in the Industry 226

6.2 Key Challenges in Using FEM for Fiber-Reinforced Polymers 227

6.3 Modeling Discontinuous Fiber-Reinforced Materials for FEM Implementation 232
6.3.1 Macro Scale or Phenomenological Modeling 233
6.3.2 Micro Scale Modeling 234
6.3.2.1 Mean Field Homogenization 240
6.3.2.2 Representative Volume Element (RVE) Using a Finite Element Approach 242
6.3.2.3 Generalized Method of Cells 244
6.3.2.4 Repetitive Unit Cell (RUC) 246
6.3.3 Multiscale Modeling 248

6.4 Survey of Existing Options in Multiscale Modeling of Fiber-Reinforced Material ... 252
6.5 Comments and Guidance ... 253
References ... 255
Appendix ... 256

7 Process Simulation for Discontinuous Fibers ... 261
Huan-Chang Tseng, Jim Hsu, Anthony Yang, Sebastian Goris, Yu-Yang Song, Umesh N. Gandhi, and Tim A. Osswald

7.1 Modeling Fiber Motion During Processing ... 261
7.2 Process Simulation ... 261
7.2.1 Injection Molding ... 262
7.2.1.1 Mathematical Models and Assumptions ... 262
7.2.1.2 Numerical Method ... 264
7.2.2 Compression Molding ... 266
7.2.3 Discussion on Key Challenges in Simulation of Compression Molding ... 268
7.2.3.1 Key Challenges in Compression Molding Simulation Using a Bulk Charge ... 273
7.2.3.2 Key Challenges in Compression Molding Simulation Using Sheet Charge ... 274
7.3 Fiber Modeling ... 277
7.3.1 Fiber Orientation ... 277
7.3.1.1 Folgar-Tucker Model ... 277
7.3.1.2 RSC Model and ARD-RSC Model ... 278
7.3.1.3 iARD-RPR Model ... 280
7.3.2 Fiber Breakage ... 281
7.3.3 Fiber Concentration ... 283
7.4 Fiber Configuration Prediction ... 286
7.4.1 Fiber Orientation and Fiber Breakage ... 286
7.4.2 Fiber Concentration ... 294
7.5 Direct Fiber Simulation ... 297
7.5.1 Application Example: Fiber Orientation Evolution during Compression Molding ... 302
7.6 Conclusions ... 305
7.7 Future Challenges ... 305
References ... 307

8 Case Studies to Demonstrate Application of Multiscale Modeling for Fiber-Reinforced Polymers 311

8.1 Study of Effect of Manufacturing Process on Flat Plaques 312
8.1.1 Plaque Manufacturing Details 312
8.1.2 Effect of Manufacturing Process on Plaque Properties 314

8.2 Multiscale Finite Element Simulation for the Fiber-Reinforced Flat Plaques 326
8.2.1 Details of the Finite Element Model 331
8.2.1.1 Process Simulation Model 331
8.2.1.2 Structure Simulation Model 334
8.2.1.3 Discussion on How to Choose the Modeling Details 335
8.2.2 Simulation Results for the Plaques 338
8.2.3 Discussion on Applying the Multiscale Simulation 341
8.2.4 Comments on Limitations of the Approach 349

8.3 Warpage Study for a Flat Plaque 350
8.3.1 Discussion on Mechanism of Warpage 351
8.3.2 Detail of the Plaques 353
8.3.3 Prediction Method Approach 355
8.3.4 Mechanical Material Properties Calculations Using Reverse Engineering 359
8.3.5 Finite Element Analysis to Calculate Warpage 365
8.3.6 Comments and Limitations 367

References 368

9 Special Topic: Compression Molding of Discontinuous Fiber Material 371

9.1 Compression Molding of Bulk Materials 374
9.1.1 Example 1: Single-Cavity Glass Fiber-Reinforced Polymer (GFRP) Part 375
9.1.1.1 Actual Part Manufacture 375
9.1.1.2 Fiber Orientation Mapping Approach 377
9.1.1.3 Mapping Algorithm 379
9.1.1.4 Demonstration of Effect of Initial Charge Orientation in the CAE Model 381
9.1.1.5 Comments and Conclusions 385
9.1.2 Example 2: Three-Cavity Carbon Fiber-Reinforced Plastic (CFRP) Sample 385
9.1.2.1 Actual Part Manufacture 386
9.1.2.2 Material Properties Measurements 387
9.1.2.3 Development of Model for CAE 388
9.1.2.4 Comparison between Simulation and Experiments 390
9.1.2.5 Comments and Conclusions 396

9.2 Compression Molding of Sheet Materials ... 396
9.2.1 Actual Part Manufacturing ... 397
9.2.2 Measurement of Material Properties of the Sheet Material ... 401
9.2.2.1 Material Structural Properties ... 401
9.2.2.2 Sheet/Mat Properties for the Mold Filling Analysis ... 402
9.2.3 CAE Simulation for the Compression Molding of Mats ... 403
9.2.3.1 Draping Analysis Using LS-DYNA ... 403
9.2.3.2 Compression Molding Analysis with Moldex3D ... 405
9.2.3.3 Comparison between Simulation and Experiments ... 406
9.2.4 Comments and Conclusions ... 410
9.3 Compression Molding of GMT Material ... 411
9.3.1 Discussion on GMT and Approach ... 412
9.3.2 Actual Part Manufacturing ... 413
9.3.3 Finished Parts Properties Measurements ... 414
9.3.4 FEA Analysis ... 417
9.3.4.1 Compression Molding Process Simulation ... 417
9.3.4.2 Non-linear Structural FEA Simulation for the Tensile and Bending Test ... 422
9.3.5 Comments and Conclusions ... 429
References ... 429

10 Special Topics in CAE Modeling of Composites ... 433

10.1 Mixed or Hybrid Fiber-Reinforced Material Modeling ... 433
10.1.1 Study Detail ... 434
10.1.2 Tensile and Bending Test Comparison ... 435
10.1.3 Finite Element Modeling for the Hybrid Material ... 437
10.1.4 Comparison of Simulation Result with the Measurement ... 439
10.1.5 Conclusion for Hybrid Material Modeling ... 441
10.2 Adhesive Joining Modeling ... 442
10.2.1 Background of Adhesive Modeling in Finite Element Models ... 444
10.2.2 Sample Preparation and Testing ... 445
10.2.3 Lap Shear Test ... 446
10.2.4 Peel Test ... 447
10.2.5 Complex Shaped Part Test ... 448
10.2.6 Modeling and Simulation ... 449
10.2.7 Lap Shear FE Model ... 451
10.2.8 Peel Test FEM Modeling ... 452
10.2.9 Complex Shaped Part FEA Modeling ... 455
10.2.10 Conclusions for Adhesive Joining ... 457
References ... 458

Index ... 461

plastic preform and over-mold them with the discontinuous fiber-reinforced material, resulting in a structural part that is much lighter, tougher, and stronger than the traditional single material steel components it replaces.

Hybrid parts have been particularly important in the automotive industry. One of the first hybrid structures was the front end of the Audi A6 in 1998, which lowered the cost by 10% and the weight by 15% [25]. In 1999, Ford introduced the hybrid front end for their Focus, making it 40% lighter and 20% cheaper than the steel part it replaced. This front end integrated steel inserts over-molded with 30% glass fiber filled polyamide 6 features. The front end is depicted in Figure 1.12.

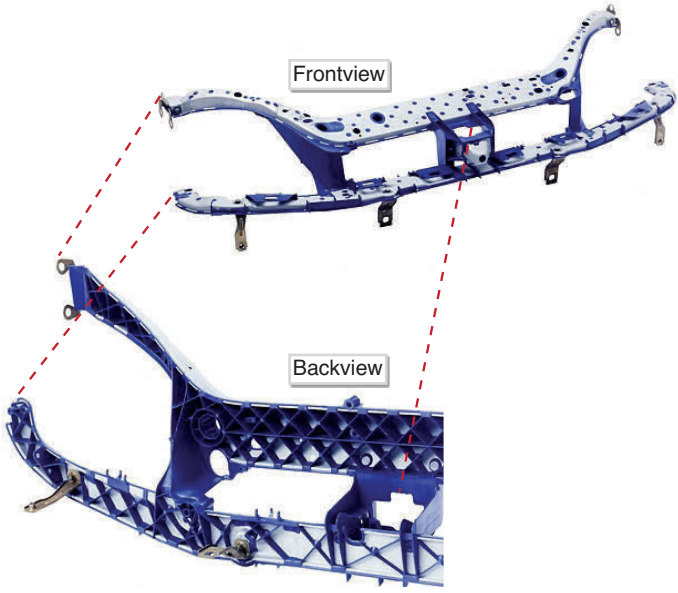

Figure 1.12 Ford-Focus hybrid front end structure made of steel inserts over-molded with 30% by weight glass reinforced polyamide 6 (Courtesy Dynamit Nobel Kunststoff)

■ 1.3 Lightweighting in Automotive Applications

In recent years, global temperatures have been rapidly rising, pushing noticeable changes in the environmental patterns and landscape, including sea levels. At this moment, the earth environment is still relatively stable. However, many scientists fear that, if the current trends continue, the environment may reach a tipping point where significant irreversible shift in the earth environment may be triggered,

causing large changes in the landscape and human disaster of unknown proportions. There are many theories on what is causing the global warming. The majority of the scientist believes that the increased emission of carbon dioxide from the fossil fuels such as petroleum, natural gas, and coal are major contributors. In the past 100 years, since the advent of industrial revolution, the use of such fossil fuels has grown tremendously (9 kTWh in 1910 to 123 kTWh in 2010) due to the increase in population and changes in the lifestyle.

Automobiles in the U.S. are considered among the largest emitters of carbon dioxide. As shown in Figure 1.13, almost 28% of greenhouse gases are coming from transportation. This directly correlates with the energy consumption in the transportation sector at 28% of the total energy consumed in the U.S., as shown in Figure 1.14. Therefore, it is imperative that we reduce the fuel consumption in the transportation industries to lower the greenhouse gases overall.

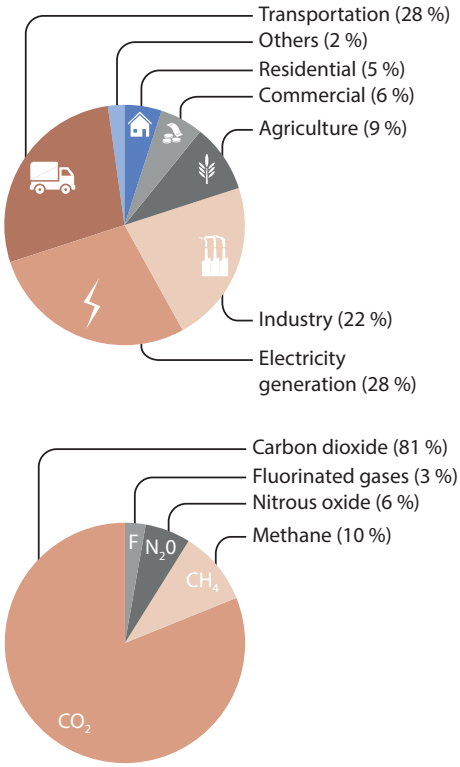

Figure 1.13 Source and breakdown of content of greenhouse gases in the U.S.; note that 28% of greenhouse gases are coming from transportation [7]

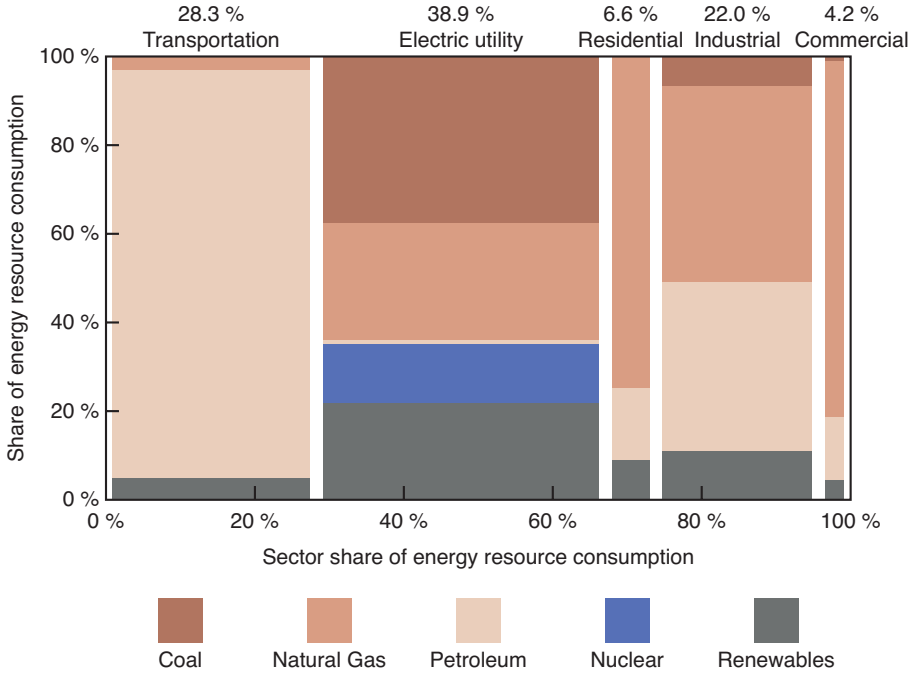

Figure 1.14 U.S. energy consumption by sector; 28% of the energy is consumed by transportation sector; most of it comes from petroleum [8]

The fuel consumption can be reduced by improving the powertrain efficiency, reducing the aerodynamic drag, and using lighter vehicles. Many studies conducted over time in the U.S. [9–11] indicate that for every 10 percent reduction in vehicle weight, fuel consumption can be reduced by approximately 4–8 percent. Actual reduction can vary based on the vehicle specifics, but the trend holds true in general. The main reason for such a direct relationship is engine size. As the vehicle weight is reduced, the power to accelerate the vehicle is also reduced; hence, smaller engines are needed. The smaller engine size becomes the key contributor in reducing the fuel consumption. When the vehicle body is made of lighter materials to reduce weight, it has cascading effects; the size and weight of auxiliary components such as brakes, wheel axles, transmission, and engine are reduced as smaller amounts of weight are supported. As a result, for an engine operating under similar conditions, it can be smaller and use less fuel. The flow of energy from fuel is presented in Figure 1.15: almost 2/3 of energy is used in the engine, while the remaining energy is used in overcoming the friction and other losses; only about 10–12 percent of the energy goes into moving the vehicles. The weight reduction is even more important for electric vehicles. This is because as the vehicle's weight is reduced the energy required to travel is also reduced, hence realizing significant improvements in the range [12].

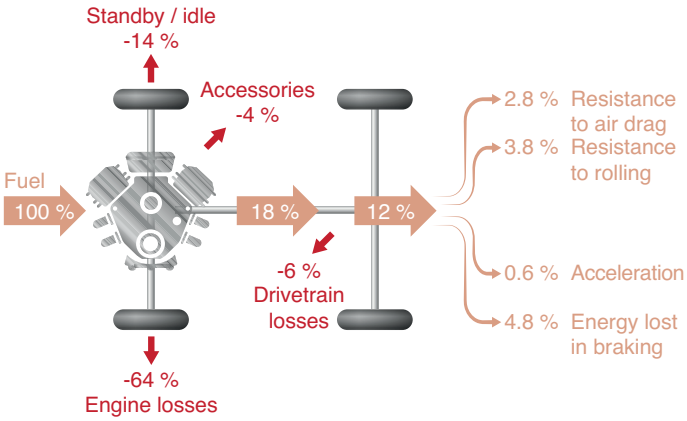

Figure 1.15 Source of fuel usage in a typical vehicle and how weight reduction can help

Therefore, weight reduction of the vehicle body structure has become one of the key focus areas. The history of a typical passenger vehicle's weight since 1975 is presented Figure 1.16. It is interesting to observe that after the fuel crisis in the late 1970s the vehicles became significantly lighter in the early 1980s and then the weight started to increase. Trends in the past 10 years show that the weight of vehicles have stabilized. If we consider the Toyota Corolla, a typical Corolla that weighed about 950 kg in 1983 increased its weight to 1350 kg in 2010. The increase in the vehicle weight was due to many safety regulations rolled out in the 1990s and 2000s, which resulted in improvements in the vehicle structure to absorb crash energy, sensors to detect the impact, and airbags to protect the occupants. These all improved safety but also added weight to the car. In addition, the demand for more comfort and entertainment has increased significantly in the past few years, resulting in larger vehicles with many comfort features and gadgets. During the same period the powertrain technology has also significantly improved. Surprisingly, the result is that the fuel consumption per mile has only increased modestly. In recent years (since 2005) we observe that the weight increase has stabilized while technology to improve fuel efficiency continues to improve; as a result, fuel economy has continued to improve [13].

2 Materials

The major components of a composite material are the reinforcing phase and the surrounding matrix. The reinforcing phase can be particles, agglomerates, platelets, or fibers. When considering fibers, they are either continuous or discontinuous while the continuous fibers can also be woven or braided. In general, the reinforcing phase is joined to the matrix with sizing materials, which depend on the type of matrix used, which can be either thermoplastic or thermosetting. This chapter will present an overview of the reinforcing phase and the matrix.

2.1 Reinforcing Phase

Composite materials are a distinctive set of materials characterized by the combination of individual components to achieve an enhanced material, which exceeds the capabilities of each individual phase. Due to the unique properties of composites, these materials are found in many industries and unique processes have been developed that correspond to the various types of reinforcement. In their most general form, composites are the result of embedding particles of one material in a surrounding matrix of another material. The combination of the particles with the matrix produces a favorable mix of properties that cannot be achieved with either of the constituents acting alone. There are many types of composite materials and Figure 2.1 presents a general classification of fiber-reinforced composites. The shape and dimensions of the reinforcing phase highly affect the mechanical properties of the composite and, in general, composite materials are classified based on the geometry of the reinforcement.

Figure 2.1 is only one way of classifying fiber-reinforced composite materials and a more general and comprehensive classification can include non-fibrous particles or hybrid compositions. Within the larger classification of fibers we can subdivide those as continuous and discontinuous fibers.

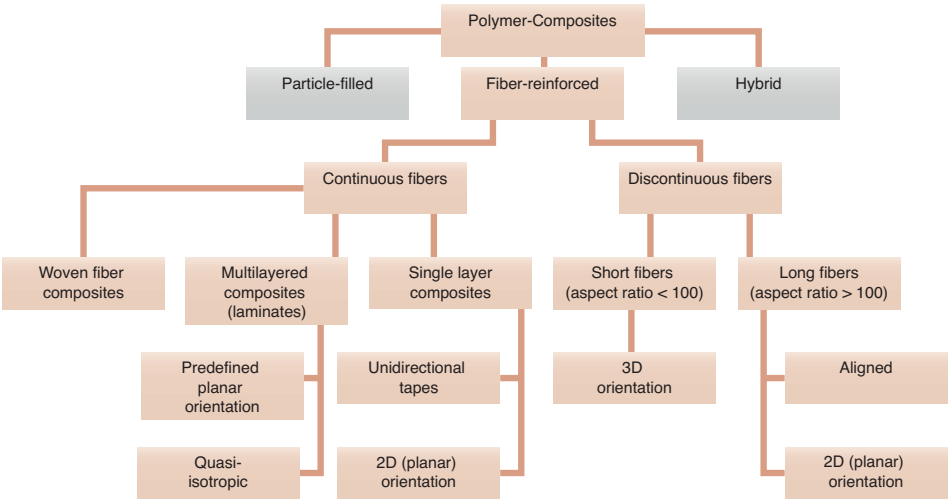

Figure 2.1 Classification of composite materials based on the type of reinforcement

2.1.1 Particle-Reinforced Composites

Particles are those reinforcing materials that do not have a long dimension and can have a spherical, ellipsoidal, obloidal, polyhedral, or even irregular shape. Particle-reinforced composites are some of the oldest types of composite materials. Particulate fillers can increase the stiffness of composite parts, but the level of reinforcement is much smaller than that of fiber-reinforced composites, as the small particles lead to stress concentrations that make the combined materials brittle. For example, a polymer that is tough in its unfilled state becomes brittle when volume fractions of the particles exceed 10% [1]. More often, particles are used to enhance properties such as thermal and electrical conductivity, surface hardness, and wear resistance. The most popular particle used in particle-filled polymers is carbon black. This inorganic filler has been used in the rubber industry since the advent of the rubber tire in the form of rubber/carbon-black composites. Carbon-black, which when dispersed is composed of 10 nm to 100 nm particles, serves not only to stiffen and reinforce rubber, but also to increase its thermal and electrical conductivity. Besides enhancing the properties of the composite, particles can be considerably cheaper than the matrix material. Thus, particles can also be simply used to reduce cost. In the field of inorganic particulate fillers, an active research area in the composites industry has emerged, which concentrates on making polymers more thermally conductive, in some cases by a factor of 100 [2]. This allows the use of inexpensive manufacturing techniques to mold particle-filled plastic parts that conduct heat out of critical automotive components, computers, and heat exchangers [3] as well as in mechatronics applications.

A new class of particle-reinforced composites, nanocomposites, has its roots in the rubber industry. By definition, nano-sized particles have at least one dimension in the nanometer scale. The nano-fillers have an exceptionally high surface to volume ratio and, compared to their bulk size equivalents, nanoparticles have significantly different properties. Nanoparticles greatly improve the properties of the composite and sometimes only small amounts of nanoparticles can lead to improved performance.

Although particle-reinforced composites are a major class of composites, the discussion in this chapter focuses on fiber-reinforced polymer composites. For a detailed discussion on particle-filled composites, the authors suggest [4].

2.1.2 Continuous Fibers

Continuous fiber-reinforced composites are used in structural applications where increased strength and stiffness are required. For example, by stacking single plies of continuous fibers, composites are often made into laminates. The fibers in each ply have a defined orientation and the arrangement of the plies is tailored to enhance the strength of the composite in the primary load directions. For continuous fiber-reinforced composites, the orientation of the fibers is pre-defined by assembling preforms and typically does not change during processing. Several identical or different layers may be bonded together, which is also referred to as *laminate*. The orientation of the fibers in each layer is designed to match the load of the final part. Such types of continuous fiber composites have been traditionally used in aerospace applications, such as in the Boeing 787 discussed in Chapter 1, as well as in lower volume production automobiles such as some panels and structural elements like the B-pillar of the R8 Audi Super sports car, also presented in Chapter 1.

Textile composite structures are an advanced subcategory of continuous fiber composites, which can even further improve the performance of a composite part. The three main types of fabric used in textile composites are: woven, braided, and knitted. Knitted fabric results from knitting of fibers. Generally, such fabrics are stretchable with low tensile and compressive properties, which makes them ideal for gloves, shoes, etc. Their usage in composites has been limited so we will focus on the other two types in the next section.

2.1.2.1 Woven Fabrics

Resin impregnated woven fabrics are widely used in hybrid structures, where they are over-molded with discontinuous fiber-filled ribbed structures. The simplest form of a woven fabric is the one that has a plain weave and is schematically depicted in Figure 2.2 (left). In a weave, the longitudinal threads are called the warp,

and the lateral threads are called the weft or the filling. A woven fabric is typically manufactured using a loom that interlaces the warp and weft yarns. The longitudinal threads, or warp threads, are held stationary and in tension, and the weft or fill is inserted over and under the warp threads.

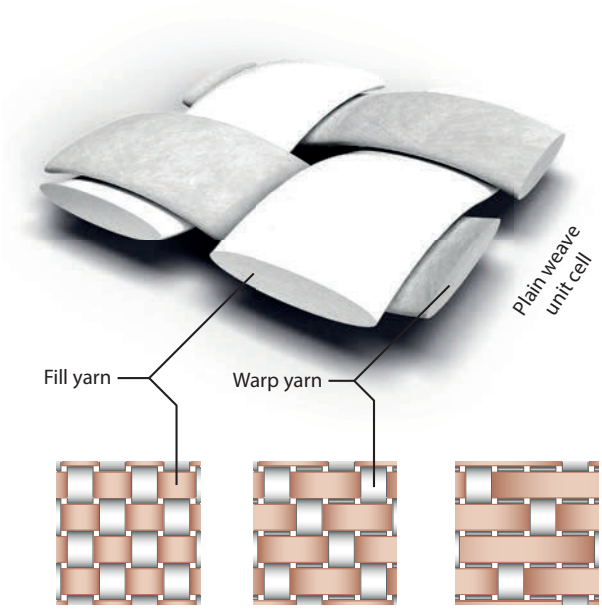

Figure 2.2 Most common types of fabrics: plain (left), twill (center), and satin (right)

Three major types of weaves are used in the composites industry [5]. These are plain, twill, and satin weave. The plain weave is the type of weave with the shortest float where warp and weft are interlaced at every intersection. In a twill fabric, the weft skips or floats over one or more warp threads. A satin is the type of fabric where the weft skips over more than four warp threads. With increasing float, the resistance to deformation decreases, which can have a negative impact when handling the fabric but can improve its drapability. This makes twills and satins more likely to take on shapes that have double curvatures. If the weave of two neighboring weft threads is shifted by one thread, a characteristic diagonal pattern is created such as shown with the twill and satin weaves in Figure 2.2 (center and right) [6].

In the manufacture of hybrid structures, woven fabrics must often be conformed to complex three-dimensional surfaces such as shown in Figure 2.3. The figure depicts an X-ray micro-computed tomography (μCT) scan as an example of a thermoplastic impregnated fabric, draped over a complex tool. As can be seen, such a draping process poses many problems such as those resulting from wrinkling and

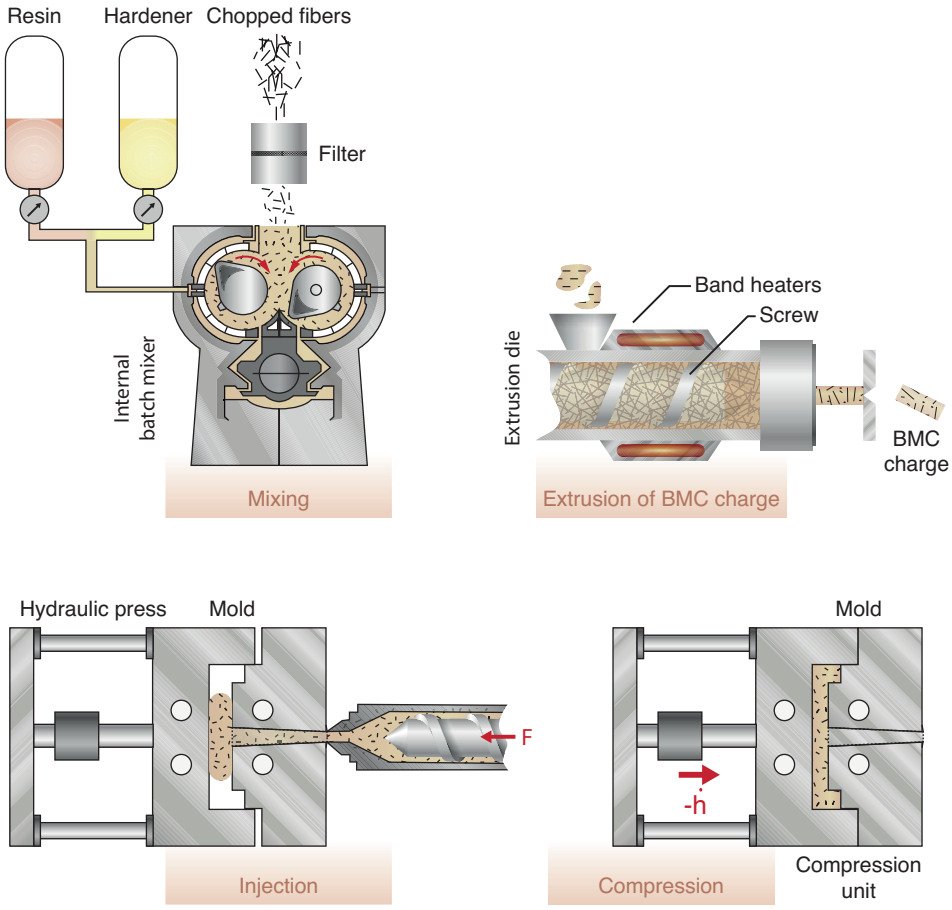

Figure 3.6 BMC injection-compression molding process

■ 3.2 Fiber-Reinforced Thermoplastics

In a thermoplastic polymer, the molecules are not cross-linked with each other. Instead, the individual molecules are held in place by weaker intermolecular forces such as van der Waals forces and hydrogen bonds. In polymer processes, thermoplastics solidify as they are cooled from the molten state and the long molecules are no longer allowed to move freely. When reheated, these materials regain the ability to "flow" and the molecules are able to slide past each other with ease. Thermoplastic polymers are divided into two classes: amorphous and semi-crystalline polymers. Amorphous thermoplastics have molecules that remain in disorder as they cool, leading to materials with a fairly random molecular structure. An

amorphous polymer hardens, or vitrifies, as it is cooled below its glass transition temperature. Semi-crystalline thermoplastics, on the other hand, solidify while forming a crystalline structure. As the material is cooled, the molecules begin to arrange in a regular order once the temperature drops below the melting temperature. However, in semi-crystalline polymers small amorphous regions remain where the molecules are not ordered. These amorphous regions within the semi-crystalline domain lose their "flowability" below their glass transition temperature. Because most semi-crystalline polymers have a glass transition temperature at subzero temperatures, they behave like rubbery or leathery materials at room temperature.

Discontinuous fiber-reinforced thermoplastics have been used in injection or compression molding for a long time. Compared to SMC or BMC, fiber-reinforced thermoplastics show advantages such as higher impact strength, lower cycle times, and recyclability. However, the high viscosity of a thermoplastic resin makes it more difficult to impregnate the fibers and the surface finish is poor compared to SMC. Different processes have been developed and several material combinations exist. Depending on the application, the matrices may be of polypropylene, polyamide, or any other engineering thermoplastic. Currently, glass fibers have the biggest market share, although the applications with carbon fibers are increasing. The following sections summarize the three main processes in discontinuous fiber-reinforced thermoplastics: injection molding, compression molding, and extrusion-compression molding.

3.2.1 Injection Molding

Injection molding is the most important process used to manufacture plastic products. Today, more than one-third of all thermoplastic materials are injection molded and more than half of all polymer processing equipment is for injection molding. The injection molding process is ideally suited to manufacture mass-produced parts of complex shapes requiring precise dimensions. The process goes back to 1872, when the Hyatt brothers patented their stuffing machine to inject cellulose into molds. However, today's injection molding machines are mainly related to the reciprocating screw injection molding machine patented in 1956. A modern injection molding machine with its most important elements is shown in Figure 3.7. The components of the injection molding machine are the plasticating unit, clamping unit, and the mold.

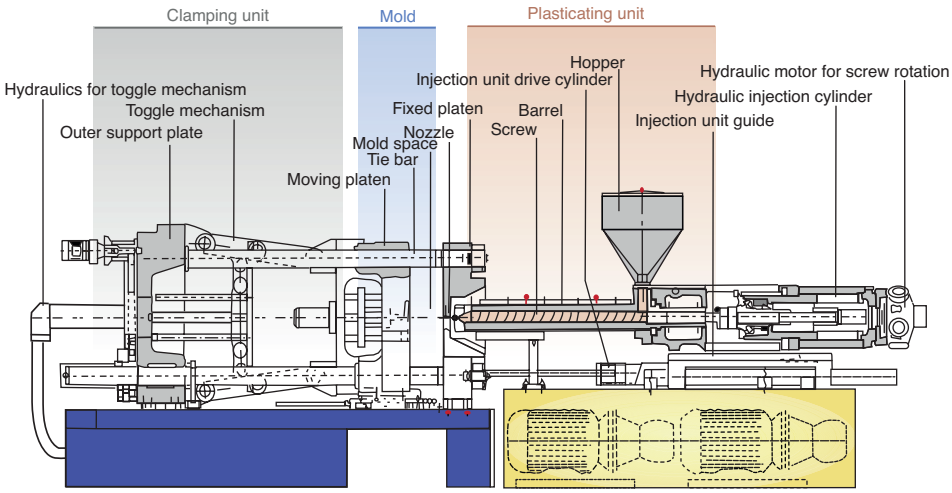

Figure 3.7 Schematic of an injection molding machine

Today, injection molding machines are classified by the following international convention[1]

$$\text{Manufacturer} \quad T / P \tag{3.1}$$

where T is the clamping force in metric tons and P is defined as

$$P = \frac{V_{\max} p_{\max}}{1000} \tag{3.2}$$

where $V_{\max}$ is the maximum shot size in cm^3 and $p_{\max}$ is the maximum injection pressure in bar. The clamping force T can be as low as 1 metric ton for small machines, and as high as 11,000 tons.

The sequence of events during the injection molding of a plastic part, as shown in Figure 3.8, is called the injection molding cycle. The cycle begins when the mold closes, followed by the injection of the polymer into the mold cavity. Once the cavity is filled, a holding pressure is maintained to compensate for material shrinkage. In the next step, the screw turns, feeding the next shot to the front of the screw. This causes the screw to retract as the next shot is prepared. Once the part is sufficiently cool, the mold opens and the part is ejected.

[1] The old U. S. convention uses Manufacturer *T-v*, where *T* is the clamping force in British tons and *v* the shot size in ounces of polystyrene.

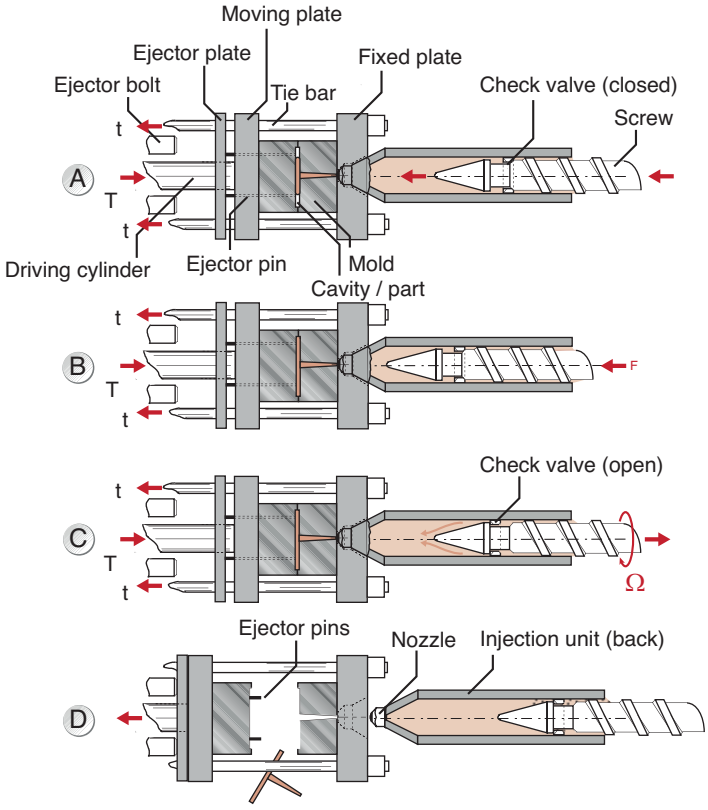

Figure 3.8 Sequence of events during an injection molding cycle

Figure 3.9 schematically illustrates the sequence of events during the injection molding cycle. The figure shows that the cycle time is dominated by the cooling of the part inside the mold cavity. The total cycle time can be calculated using

$$t_{\text{cycle}} = t_{\text{closing}} + t_{\text{cooling}} + t_{\text{ejection}} \tag{3.3}$$

where the closing and ejection times, t_{closing} and t_{ejection}, can last from a fraction of a second to a few seconds, depending on the size of the mold and machine. The cooling times, which dominate the process, depend on the maximum thickness of the part. The cooling time for a plate-like part of thickness h can be estimated using

$$t_{\text{cooling}} = \frac{h^2}{\pi\alpha} \ln\left(\frac{8}{\pi^2}\frac{T_m - T_w}{T_D - T_w}\right)$$

and for a cylindrical geometry of diameter D using

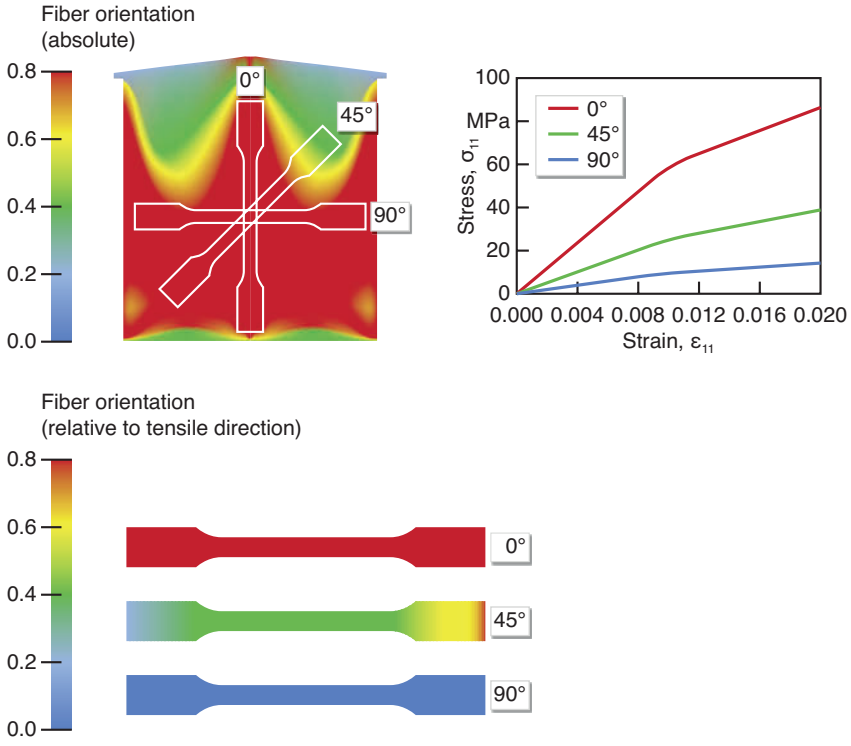

Figure 4.14 Illustration of the process-induced fiber orientation, obtained from a basic process simulation of a fan-gated plaque. The impact of fiber orientation, caused by the mold filling, is shown for specimens extracted at 0, 45, and 90 degrees

For a more detailed discussion on process simulation, the reader should consult Chapter 7 of this book. Furthermore, the effect of process-induced microstructure on the mechanical properties within a plaque is investigated in detail in Chapter 8.

■ 4.2 Characterization Techniques for Fiber Microstructure Analysis

Quantifying the process-induced fiber configuration in molded samples is of utmost importance so that the underlying physics of the process–microstructure relationship can be studied experimentally. Furthermore, accurate and reliable experimental data are required to test and develop numerical models and predictive tools. At times, the lack of accurate experimental data limits the progress of validating modeling approaches [2, 6]. Nevertheless, the characterization of fiber configuration is a cumbersome task since even small samples comprise millions of fi-

bers. A wide variety of measurement approaches exist, but no standard has been accepted nor has a uniform procedure been defined. While some measurement concepts share similarities, there are substantial differences in key aspects of the measurement techniques and the execution of the actual measurements. The following sections provide an in-depth review and discussion of measurement techniques used to quantify the orientation, length, and concentration in discontinuous fiber-reinforced polymers.

4.2.1 Measuring Fiber Orientation

For decades, fiber orientation measurements were performed manually by physically sectioning the sample and inspecting the cross sections using optical reflection microscopy [45–47], which is referred to as the method of ellipses (MoE). The fibers leave elliptical footprints on the polished cross sections, which are detected and analyzed for individual fibers. The fiber orientation can be quantified by analyzing the shapes of the ellipses, as illustrated in Figure 4.15. An image analysis system imports the captured micrographs and fits ellipses to determine the angles ϕ and θ individually for each fiber [47]. Although newer systems are automated to a degree, this technique still requires a lot of manual work to achieve accurate results. Furthermore, the destructive nature of this method does not allow additional testing of the sample, e.g., fiber length analysis. Moreover, the two-dimensional observation of the ellipses results in ambiguity with respect to the out-of-plane angle θ, because the fiber can be oriented at θ or $\theta+\pi$, as illustrated in Figure 4.15. However, this ambiguity can be resolved by an additional etching after each polishing step, so that a fiber's shadow is visible in the micrograph. By determining the location of the shadow relative to the corresponding fiber, the angle θ can be distinctly defined [32].

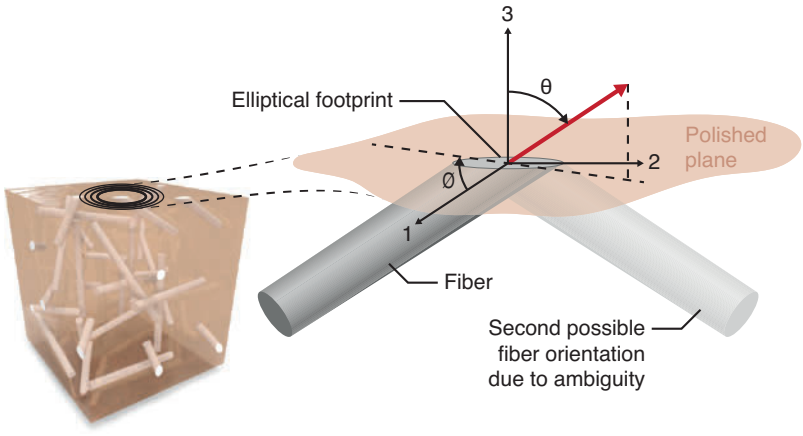

Figure 4.15 Basic principle of the method of ellipses and illustration of the ambiguity in the out-of-plane angle θ

A relatively new approach to measure fiber orientation distribution within fiber-reinforced plastic parts is applying the X-ray micro-computed-tomography (μCT) technology. This technique is a non-destructive testing (NDT) method, which enables a full 3D analysis of a specimen and the quantification of internal material structure [48–50]. The advantage of μCT is that it can achieve high resolution of the full 3D microstructure without destroying the specimen. Originally, μCT was solely used in medical applications, but it has now evolved to be a conventional characterization technique in the material sciences and in industrial applications. A basic schematic of the μCT process is illustrated in Figure 4.16.

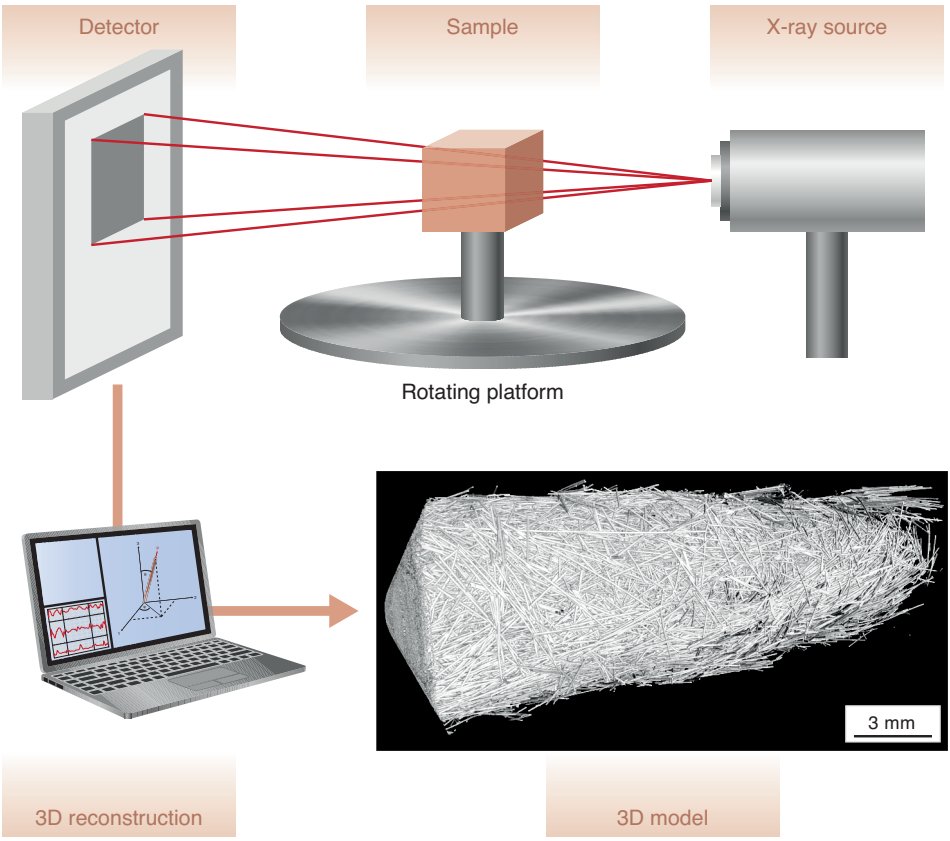

Figure 4.16 Illustration of the X-ray computed-tomography process: the μCT system comprising the detector, X-ray source, and rotating platform (top), the computer-assisted tomographic reconstruction (bottom left), and a 3D rendering of the data reconstruction (bottom right)

In general, the system consists of an X-ray source, a rotating platform and a detector. The basic principle of μCT is to irradiate a sample with penetrating X-rays, which are attenuated and captured downstream of the object with a detector system creating radiographs. At defined energy levels, the X-ray source irradiates the

specimen, which is placed on a rotating platform to achieve a full scan of the sample. The detector records the attenuated X-rays as radiographs at incremental angles during the rotation of the sample. Each captured projection (radiograph) is a two-dimensional intensity distribution of the attenuated X-rays. The intensity distribution is directly related to the material's atomic density. A phase of high atomic density within the specimen absorbs more energy than low-density materials.

The X-rays interact with the sample and are attenuated in various ways. For the energy range of the X-rays used in material science, the most relevant mechanisms are Compton scattering and photoelectric effects [48]. Most fundamentally, the attenuation of an X-ray through a sample can be described by the change in intensity I as

$$dI = -\mu_{eff}(x)I(x)dx \tag{4.11}$$

where μ_{eff} is the effective linear attenuation coefficient and x is the location on the path. Integration of Equation (4.11) along the path C gives

$$-\ln\frac{I}{I_0} = \int_C \mu_{eff}(x)dx \tag{4.12}$$

which is also referred to as the Beer-Lambert law. Computing the correct value of μ_{eff} at each position along the path C is the central problem of computed tomography, called tomographic reconstruction. Several approaches and algorithms exist for the reconstruction and the reader is directed to [48] for more detailed information.

After the completion of the 3D reconstruction, the μCT data set can be further processed for qualitative and quantitative analysis of the actual specimen. Different software and algorithms exist to process the μCT images and analyze the fiber orientation distribution. A major challenge in using μCT for fiber orientation analysis is the amount of data that is generated, which has to be post-processed to quantify the orientation. For example, a scan of a 20 × 20 × 3 mm^3 sample at a resolution of 10 μm results into 8 GB of data. There are software packages from the medical field, e. g., Mimics® (Materialise NV, Belgium) that are adapted to be used for fiber orientation analysis [51]. Another software package for material science and industrial application is VG Studio MAX (Volume Graphics GmbH, Heidelberg, Germany), which also has a module for fiber orientation analysis and quantifies the fiber orientation using the structure tensor approach [52]. It was shown that VG Studio MAX provides fast and accurate μCT data analysis, making it the most commonly used software for fiber orientation measurements at the moment [53]. Additionally, research groups frequently develop their own image processing algorithms to quantify the fiber orientation from μCT scans.

The resolution (voxel size) of the scan is one of the most important parameters that determine the accuracy of the feature analysis of scanned samples. However, the trade-off between scan resolution and sample size needs to be considered. In general, finer scan resolutions require samples with smaller dimensions. Although a very fine resolution might be needed for an accurate analysis, a small sample might not fully represent the local orientation, especially for long fiber-filled materials. It has not been established what the minimum resolution might be to perform an accurate fiber orientation analysis for a specific fiber type. Furthermore, μCT scanning is limited in the case of composite materials with constituents that have similar atomic densities (e.g., carbon fiber-reinforced polyamide) since the contrast of the constituents in the radiograph is low and identifying the fibers can become challenging [80].

There is a wide variety of analysis resolution and sample size used in the microstructure analysis of fiber-reinforced samples throughout reported studies. The sample dimensions range from 3 μm voxel size resolution (sample size: 4 mm disk with a thickness of 4 mm) [54] up to a voxel size of 40 μm (sample size: 40 mm × 40 mm × 30 mm) [55]. To provide the reader an overview of recently published studies that apply fiber orientation measurements, Table 4.1 summarizes the imaging technique, sample size, and resolution used in their work.

Table 4.1 Overview and Summary of Fiber Orientation Measurement Techniques Applied in Recently Published Studies

Material	Imaging Technique	Sample Dimensions	Resolution	Reference
PP/GF	μCT	3 × 3 × 3 mm^3	8.0 μm	[56]
PA66/GF	μCT	3 × 3 × 3 mm^3	2.5 μm	[57]
PP/GF	μCT	16 × 16 × 3 mm^3	6.0 μm	[33]
PA6/GF	μCT	4 × 4 × 2 mm^3	1.4 μm	[49]
PA66/GF	μCT	10 × 10 × 2 mm^3	6.5 μm	[58]
PA6/GF	μCT	3.6 × 3.1 × 3.9 mm^3	9.0 μm	[59]
Natural Fibers	μCT	6 × 6 × 3.5 mm^3	7.8 μm	[60]
PP/GF	μCT	n/a	8.1 μm	[61]
PA66/GF	μCT	5 × 20 × (1 to 3) mm^3	6.0 μm	[62]
PP/GF	μCT	Ø 4 mm and 4 mm thickness	3.3 μm	[54]
PA6/GF	μCT	Ø 4 mm and 4 mm thickness	1.8 μm	[63]
PA/GF	μCT	Ø 4 mm and 4 mm thickness	0.7 μm	[64]
PA6/GF	Cross-sectional polishing and μCT	3.2 × 4 × 15 mm^3	9.0 μm	[65]
PP/GF	Cross-sectional polishing	1.5 × 2 × 1.7 mm^3	0.24 μm	[66]
PP/GF	Cross-sectional polishing	2 × 2 × 0.7 mm^3	n/a	[67]

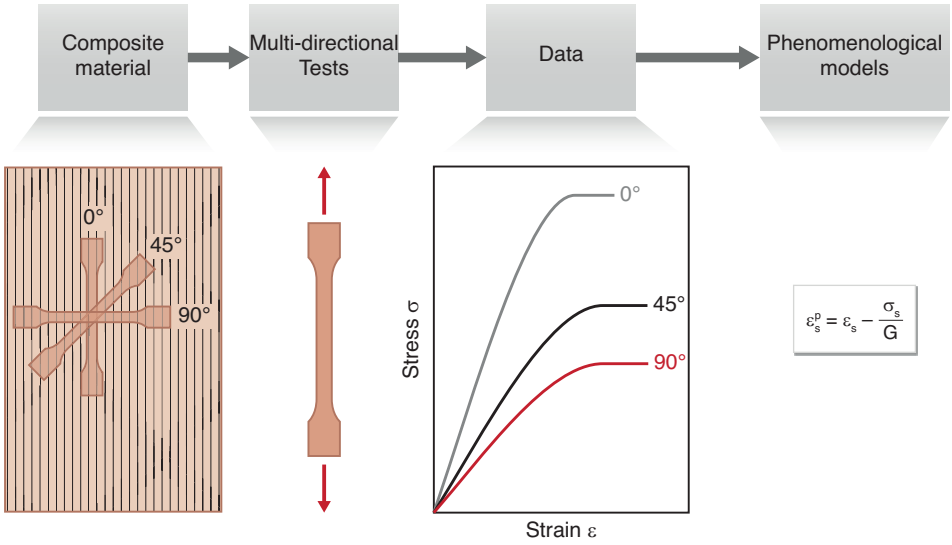

Figure 6.6 Macro scale approach to modeling

6.3.2 Micro Scale Modeling

A cross section of glass fiber-reinforced polymer composite magnified under a microscope is presented in Figure 6.7. As mentioned above, glass fibers are between 14 and 20 μm in diameter and carbon fibers are between 5 and 7 μm in diameter. In a small volume of one cubic millimeter, depending on length and volume concentration, one can expect thousands of fibers. Each of the constituents of the composite plays an important role in the final performance of that material. Particularly, for discontinuous fiber composites the fiber length, fiber alignment, fiber concentration, and fiber geometry vary from location to location and affect the final material properties within that space. If the fibers are random, evenly distributed, and are similar in length, the macro approach will work reasonably well for small deformations in the linear elastic regime. However, within the nonlinear behavior it would be very difficult to model the material behavior accurately. Also, it is imperative that the stress and strain field will be discontinuous due to the non-homogeneity of the material. This means that the damage initiation and failure estimates will be extremely difficult. Hence, microscopic models must be considered.

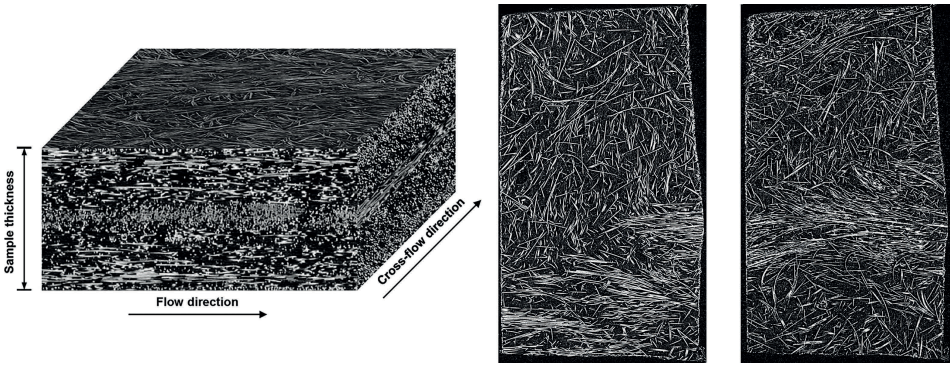

Figure 6.7 Glass fiber and polypropylene resin microstructure

With the micro scale model, ideally, one would like to account for each constituent of the composite material, i.e., fiber, resin, the interface, and their geometrical arrangements. A finite element model of the microstructure that includes all the fibers with their accurate geometry and matrix with voids can be considered. However, there are thousands of fibers even in one cubic millimeter. Modeling each fiber can result in a very large number of elements in the model, which brings computational challenges. Additionally, any constants such as interface properties are not well known. Such models, which we call a microscopic model in the true sense, are considered impractical for any useful engineering application. Many schemes to address these challenges and simplify the computational model development have evolved over time. These are called multiscale modeling. Multiscale modeling essentially incorporates the fiber details at a micro level (micrometer) and translates it into material models at macroscopic level (millimeter). There are many different schemes available to convert the microscopic details to macro level material data to be used in a finite element model.

The basic principle of multiscale modeling is presented in Figure 6.8. There, the concept of representative volume element (RVE) is used. RVE is the smallest volume which can accurately capture the structural behavior of the effective properties of the composite material. In nature, most of the structures are heterogeneous, and when dealing with such heterogeneous materials it is common to average out the effect of microstructure over a selected volume and call it effective properties. The size of such representative volume element can be debated. If the microstructure is periodic, such as with woven or layered continuous fibers, choosing the size of the RVE is easy. However, for discontinuous fibers it can be challenging. We would like the volume to be as small as possible, to capture the effect of material variation throughout the part; on the other hand, it should be large enough to average the effective composite properties as a continuum material. Generally, it is expected to be of an order of magnitude larger than the microstructure details being averaged [24].

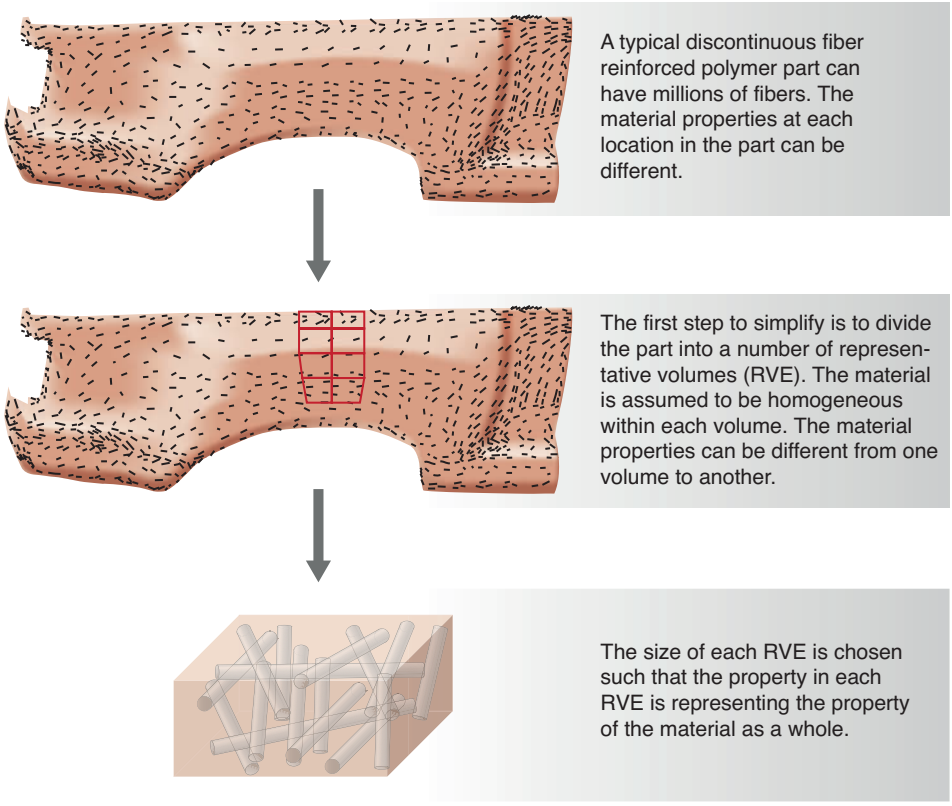

Figure 6.8 Representative volume element (RVE) concept: the part is divided into small volumes; each of them can represent the material model based on the microstructure. In FEM each such RVE can be a single finite element

The fiber-reinforced composite part can be divided into a number of representative volume elements (RVE). The constitutive material model for each RVE can be computed individually based on the fiber and resin properties and geometry details of the fibers such as fiber length, orientation, and concentration. There are many approaches to the computation of material properties in a RVE. The simplest computation is when the material properties for the RVE are assumed to be homogeneous and the averaged homogeneous material properties are used for the RVE in the finite element calculations. It is important to emphasize that, when the material properties for an RVE are assumed to be homogeneous, they can and are likely to be anisotropic for discontinuous fiber-reinforced composites. Hence, compared to the macroscopic approach discussed above, where the whole part was assumed to be homogeneous, with the RVE approach one breaks the part down into many smaller volumes at macro scale. While each of such volumes is assumed to be homogeneous, the properties from one volume to the other are expected to vary. The gross properties at whole part level can be quite different from the RVE (macro

level) properties. Also, an RVE approach better represents the actual conditions in the material. Therefore, this can be a significant improvement in the overall material property representation in the FE model.

The representative volume element approach helps significantly in reducing the computation time as well as the modeling burden. The accuracy and computational cost of such an approach depends on how the representative volume is chosen and the method used to represent the stress and strain within that volume. Furthermore, once the finite element model is used for computation, the stress and strain estimated over the RVE must be interpreted. This is important since the microstructure which is assumed to be homogeneous over the RVE is heterogeneous, consisting of the fiber and polymer resin. Depending on the fiber geometry as well as the material properties of the fibers and resin, the stress and strain in the RVE will not be homogeneous but vary from location to location. The average stress based on the homogeneous material will not be accurate. Therefore, it will be important to be able to translate the average stress and strain to a meaningful stress and strain distribution within the RVE, based on the microstructure.

Since most of the materials found in nature are heterogeneous, with two or more distinct materials at a microstructure level, the concept of using a representative volume element is widely accepted in physics. As shown in Figure 6.9, there are many different schemes developed over the years to deal with the representative volume elements for fiber-reinforced materials. Each approach has its advantages and disadvantages. The selection of a representative volume element, for a given problem, is made based on the knowledge of the microstructure, available computing resources, and level of accuracy desired. In the following sections, various methods to define the RVE for fiber-reinforced materials will be discussed. To maintain the focus of this book, the key aspects and insights will be presented from a practical perspective. Detailed theoretical background and computational derivations can be found in many references [12, 13].

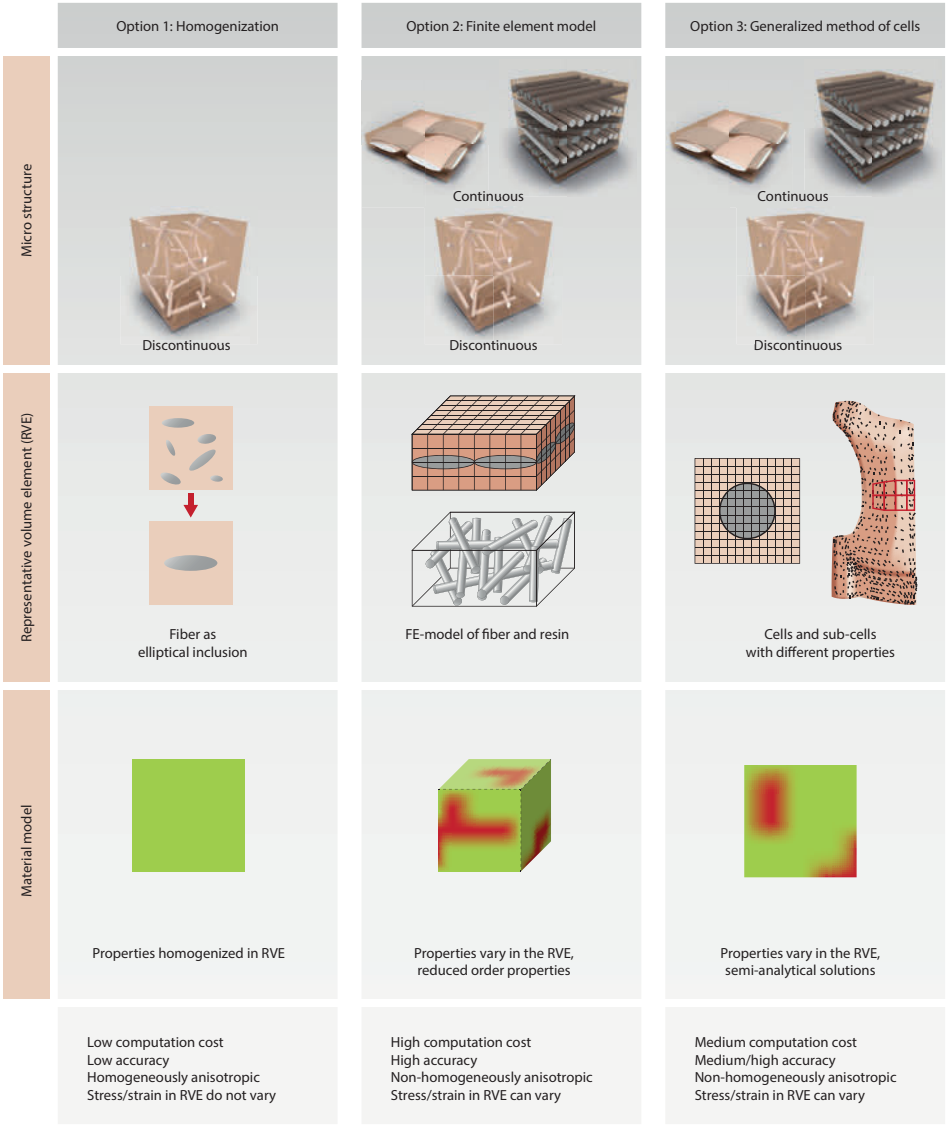

Figure 6.9 Methods to compute material properties based on microstructure for a representative volume element (RVE) for fiber-reinforced polymer composites

How a RVE can be used to generate microstructure based material properties of a fiber-reinforced composite for use with finite element analysis is presented in Figure 6.10. The key microstructure for the fiber-reinforced composite that affects the material properties are fiber length, fiber orientation, fiber concentration, fiber resin interface, and voids in the resin material. Such microstructure for discontinuous fibers is likely to vary from one location to other based on the manufacturing

8.1 Study of Effect of Manufacturing Process on Flat Plaques

In Chapter 3, different manufacturing processes were discussed, such as injection molding and compression molding, which are used to manufacture parts made of discontinuous fiber-reinforced polymers. It was also observed in Chapter 4 that the microstructure, i.e., fiber orientation, length, and concentration, in the finished part depends on the manufacturing process used. The purpose of this section is to demonstrate the effect of manufacturing methods on the material properties of a simple flat demonstrator plaque. Two different materials mixes, 30% GF (glass fiber) + PP (polypropylene) and 40% GF+PP, were used to manufacture the large plaques using many different manufacturing methods. Tensile and bending tests were conducted on the coupons from the plaques to compare their structural properties at selected locations. Furthermore, the microstructure details, such as fiber length and fiber orientations in the plaques, are measured and used to relate to material properties.

Next, the simulation of the manufacturing process is carried out to estimate the microstructure, i.e., fiber orientation and fiber length. Finally, a material model based on the fiber conditions, i.e., microstructure of the plaque is estimated. The microstructure based material models are used with the multiscale finite element model to estimate the tensile and bending performance of the samples taken from the plaque. Thus, we will show the effect the manufacturing process has on the microstructure as well as structural properties of a plaque molded for a given material. In addition, we will also show how a multiscale finite element model that accounts for microstructure helps in capturing the manufacturing effects in the FE analysis. Going through these exercises will illustrate the discussion in Chapters 6 and 7. It will also help in understanding of the multiscale modeling method for the fiber-reinforced materials.

8.1.1 Plaque Manufacturing Details

A large plaque as shown in Figure 8.1 was designed and the tool was built in such a way that it can be used to build parts using different manufacturing processes. The following manufacturing processes were used to build the parts:

- Injection molding,
- Injection-compression molding, and
- Compression molding.

Furthermore, multiple materials were used for each manufacturing process. A 30% glass filled polypropylene (30% GF+PP) and a 40% glass filled polypropylene (40%

GF+PP) were prepared using in-line compounding as well as in the pellet form. The pellets were manufactured using pultrusion as well as an extrusion (wire coating) process. Based on the different combination of materials and manufacturing processes, as shown in Table 8.1, nine different types of plaques were manufactured. The main purpose behind making these plaques, produced using different manufacturing methods, was to understand the difference in mechanical properties of the finished plaque's material, based on the manufacturing process used.

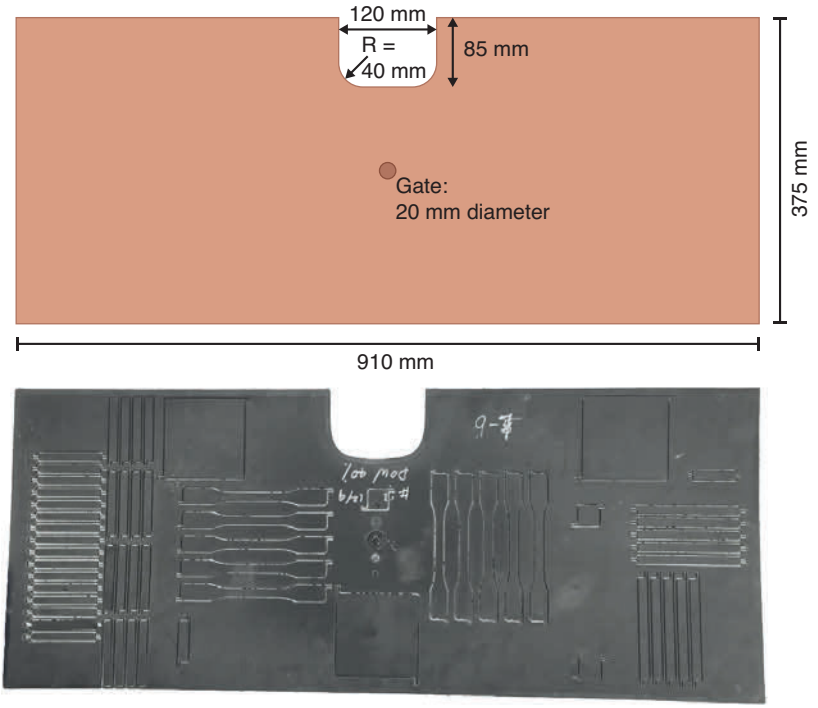

Figure 8.1 Plaque geometry and actual part used for the study

Table 8.1 Plaques Types Built Based on the Material Format and Fiber Content; the Number in Parentheses Indicates Plaque Number, Referred to in the Discussion

Manufacturing process	Material format	Glass fiber % by weight
Injection molding	In-line compounding, 15 mm long fiber	30% (2) and 40% (1)
Injection-compression	In-line compounding, 15 mm long fiber	30% (4) and 40% (3)
Compression molding	In-line compounding, 30 mm or smaller long fiber	30% (5) and 40% (6)
Injection molding	Pellet extruded	30% (7) and 40% (8)
Injection molding	Pellet pultruded	Only 40% (9)

8.1.2 Effect of Manufacturing Process on Plaque Properties

The samples for testing were cut from the plaques as shown in Figure 8.2, using a water jet cutting process, and then evaluated for tensile strength as well as bending and impact performance. Water jet cutting was used to minimize cutting related damage on the samples at the edge.

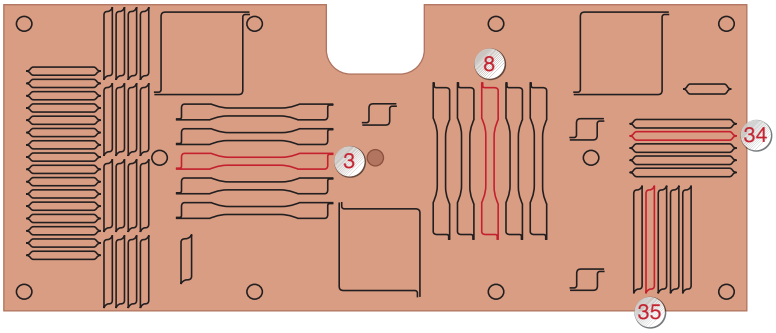

Figure 8.2 Pattern used to cut the samples for tensile and bending tests from the plaques; samples 3 and 8 are tested for tensile properties and samples 34 and 35 are tested for bending properties

The test setup used for the tensile test is presented in Figure 8.3 and that for the bending test is presented in Figure 8.4. The specimen preparation and testing are based on ISO standards for the fiber-reinforced plastics.

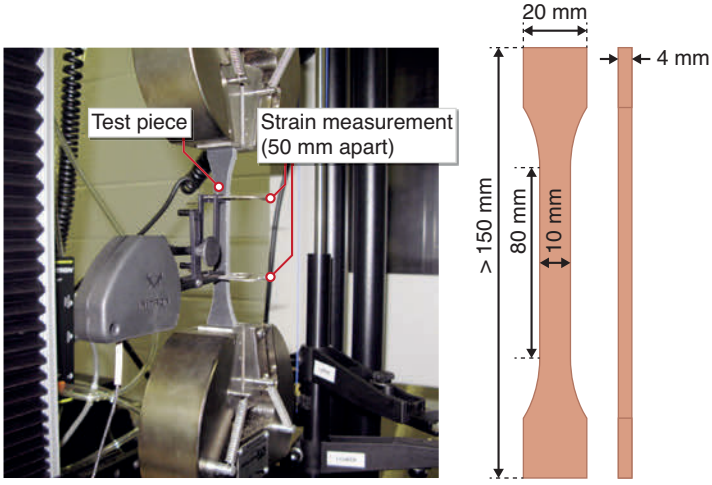

Figure 8.3 Test setup for tensile test

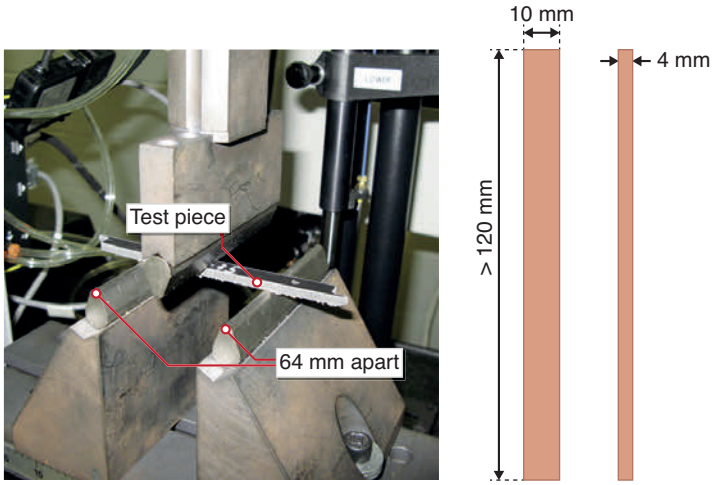

Figure 8.4 Test setup for bending test

The stress–strain curves for different plaques computed for individual test specimens are compared in Figure 8.5. Force deflection measured for the three-point bending test specimens are compared in Figure 8.6. Since plaques are likely to have variations from one to another, three samples were tested and the sample with median values of the three is used for comparison. The peak values of stress and strain at failure for the tensile test and calculated flex modulus for the three-point bending test are presented in Table 8.2. In this study, the term longitudinal is used for samples aligned along the length of longer side and transverse is used for samples aligned along width of the shorter side of the plaque, as depicted in Figure 8.5 to Figure 8.8. It is understood that the melt enters at a single point in the center and flows radially to fill the plaque cavity. However, because of the plaque geometry more material flows along the longitudinal direction. Therefore, it can be considered as *flow direction* and the corresponding transverse direction as *cross-flow direction*.

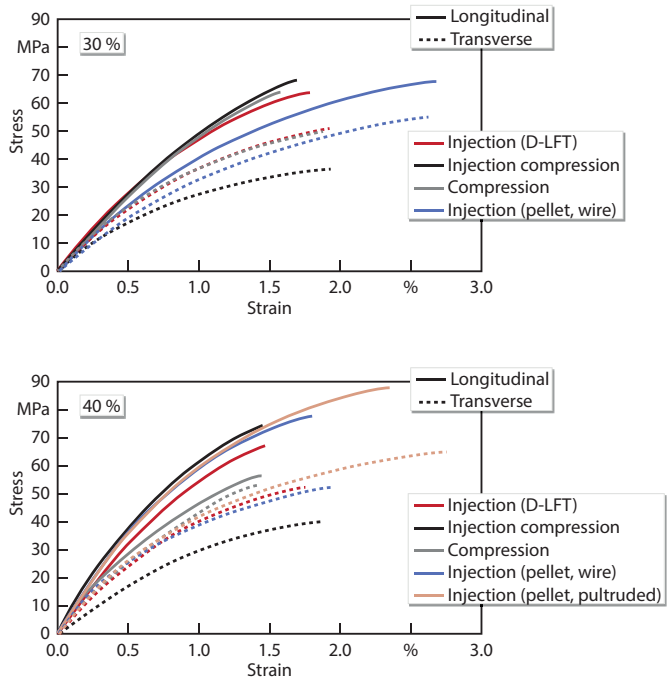

Figure 8.5 Comparison of 30% GF+PP and 40% GF+PP in the tensile test for different processes in longitudinal (L: flow) and transverse (T: cross-flow) directions; samples 3 and 8 in Figure 8.2

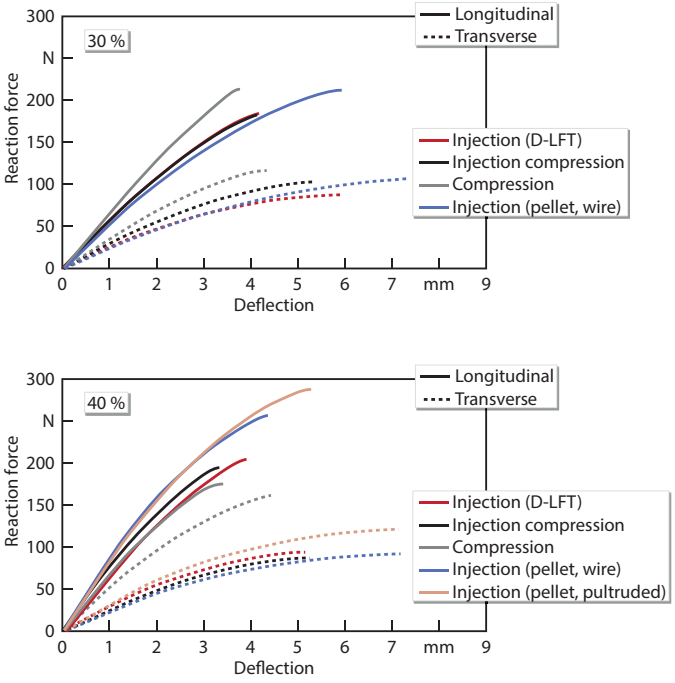

Figure 8.6 Comparison of 30% GF and 40% GF in bending test for different processes in longitudinal (L: flow) and transverse (T: cross-flow) directions; samples 34 and 35 in Figure 8.2.

Index

Symbols

3D printing 80
µCT 117

A

additive manufacturing 80
adhesive joining modeling
– hybrid materials 442
Advani-Tucker orientation tensors 103
Advani-Tucker tensor 278
Airbus 7
aminoxypropyltrimethoxysilane 36
anisotropic rotary diffusion model 279
ARD-RSC model 278
Arrhenius 55
ASTM-D4440 387
ASTM-D5930 387
ASTM-E1269 387

B

Baekeland, Leo 4
Bakelite 4
bending test 315, 417, 435
B-matrix 224
Boeing 7
Bois durci 2
braiding 33
Bucky Badger 205
bulk charge 372
– twin-screw extruder 376
bulk molding compound 64

C

CAE model 388
CAE modeling 433
CAE simulation
– compression molding of mats 403
case studies 311
center-gated disk 287, 294
charge
– bulk-shaped 373
– sheet- or mat-shaped 373
clamping force 67
coated fiber bundles 11
coefficient of the linear thermal expansion 272
compliance tensor 184
composites
– continuous fiber-reinforced 31
– discontinuous fiber-reinforced 34
– particle reinforced 30
– woven fabric reinforced 31
compression molding 266, 302, 312, 371
– analysis 405
– bulk charge 273
– bulk materials 374
– GMT material 411
– sheet charge 274
– sheet materials 396
– sheet molding compound 60
compression resin transfer molding 90
computed-tomography 117
constant strain triangle 221
continuous fibers 7, 227
continuous fiber tapes 434
continuous tapes 227
core-shell orientation 74, 102
co-rotational derivative 271
Corvette 6
Couette flow
– migration 285
critical fiber length 193, 196
cross-laminate 190
Cross model
– modified 264
C-RTM 90

CT scan 274, 377
– fiber orientation 400
cumulative fiber distribution 99
cumulative length distribution 98
cumulative length-weighted distribution 98
cure kinetics 54
curing reaction 50
– heat activated 48
– mixing activated 48

D

derivative
– co-rotational 271
– Jaumann 271
– operator 224
– substantial 271
DiBenedetto equation 56
differential scanning calorimeter 51
direct fiber simulation 297
discontinuous fibers 7, 227
dispersion chamber 138
displacement vector 220
D-LFT 76
down-sampling 137
draping 275
draping analysis 403
DSC 52

E

element stiffness matrix 224
ellipses method 116
energy consumption 14
epoxy 50
ethylene monomer 38
excluded volume forces 298
extrusion compression molding 76

F

fabric
– failure 213
FDM 264
FEA structural analysis 417
FEM 264
FEM analysis 219
FFF 82
fiber alignment 101
fiber attrition 96, 281
fiber attrition model 281
fiber bending 301
fiber breakage 281
fiber bundle 129, 152
fiber concentration 283, 294
fiber concentration distribution 155
fiber density 106
fiber-fiber contacts 298
fiber-fiber interaction 97, 298
fiber interactions 298
fiber jamming 110
fiber length 394
– number-average 97
– weight-average 97
fiber length distribution 97, 154, 281
fiber length measurements 129
fiber-matrix bonding 110
fiber-matrix separation 106, 283
fiber migration 283
fiber-mold interactions 97
fiber orientation 74, 101, 277
– distribution 63, 154, 197
– evolution 302
– mapping 377
– measurement 287, 400
– prediction 357
– tensor 395
fiber pull-out 171
fiber-reinforced composites
– continuous 7
– discontinuous 7
fiber-reinforced materials 371
fiber-reinforced thermoplastics 65
fiber spray-up molding 83
fiber straw 2
fiber–wall contacts 298
finite difference method 264
finite element analysis
– warpage 365
finite element method 217, 264
finite element modeling
– adhesion 455
– adhesive joining 444
– complex part 455
– hybrid materials 437
– hybrid structures 455
– lap shear 451
– peel test 452
finite element simulation
– multiscale 326
finite volume method 264
first-order autocatalytic reaction 54
first-order reaction 54
flex modulus 319
flow front 164
Folgar-Tucker model 277
force vector 220
Ford, Henry 5
fountain flow effect 75, 263
fuel consumption 14

fused filament fabrication 82
FVM 264

G

gating systems 74
generalized method of cells 244
GFRP part 375
Giesekus model 272
glass bead 108
glass mat-reinforced thermoplastics 78
GMC 244
GMT 78
GMT material 411
Gol'denblat-Kopnov model 200
greenhouse gases 13

H

Halpin-Tsai model 181, 183
hand-layup molding 84
heat capacity 387
Hooke's law 220
hybrid materials 433
hybrid structure 12, 93, 433
hydrodynamic effects 97
hydrodynamic forces 298

I

iARD-RPR model 280
initial charge orientation 381
injection-compression molding 312
– bulk molding compound 64
injection mold 72
injection molding 66, 262, 312
interaction strength tensor 207
interfacial shear strength 110
ISO-17744 standard 387

J

Jaumann derivative 271

K

Kamal-Sourour model 55
Kunc correction 133

L

laminate 179
lap shear test 446
length
– distribution 97, 281
– number average 281
– weight average 281
LFT 76
LFT-G 76
light construction
– Leichtbau 6
lightweighting 12
long fiber-reinforced thermoplastic 76
long fiber-reinforced thermoplastic granulates 76
longitudinal modulus 181

M

Malmeister model 200
manufacturing processes 59
mapping
– fiber orientation 377
material properties measurements 387
mathematical models 262
matrix
– thermoplastic 37
– thermoset 47
matrix–fiber separation 283
maximum stress at failure 318
maximum stress failure criterion 201
Maxwell model
– co-rotational 271
– generalized 272
mean field homogenization 240
measuring fiber concentration 145
measuring fiber density 145
measuring fiber orientation 116
mechanical properties 113
mechanics of composites 177
method of cells 244
method of ellipses 116
micro-CT 117
microstructure 95
– characterization 115
– fiber alignment 101
– fiber density 106
– fiber length 96
– fiber orientation 101
microstructure-property relationship 111
Mimics® 122, 125
minimum volume fraction 200
mixed materials 433
mixed structures 433
mixing rule 183

modeling
– macro scale 234
– micro scale 234
– multiscale 248
modeling and simulation 217
– adhesive joining 449
modulus 44
MoE 116
mold-fiber interactions 97
mold filling analysis 402
mold filling simulation 357
molding cycle
– GMT 80
– injection molding 69
– sheet molding compound 62
molding diagram 71
molecular weight 40
Mori-Tanaka homogenization 242
Morris and Boulay model 284
moving mesh boundary technique 267
multiscale modeling 248, 253, 311
multiscale simulation 326, 342

N

non-dispersed fiber bundles 128

O

organosilane 36
orientation ambiguity 116
orientation tensor 103, 278
Osswald-Osswald model 200

P

paperboard 212
particle level simulation (PLS) 297
peel test 447
pellets
– long fibers 11, 35
– short fibers 11, 35
Phelps-Tucker model
– fiber attrition 281
phenol-formaldehyde 48
Pinho model 200
plasticizing 100
polyethylene 38
polypropylene 46
press
– hydraulic 3
processes
– extrusion compression molding 76
– fiber-reinforced thermoplastics 65
– GMT 78
– injection molding 66
– thermoset molding 59
– vacuum bagging techniques 83
process simulation 261, 331
Prony series 272
pseudoplasticity 41
Puck model 200
pull-out 171
pultruded fibers 11
PvT curve 387
PvT diagram 69

R

radial flow expansion 75
ramp effect 87
reduced strain closure model 278
repetitive unit cell 246
representative volume element 236
resin transfer molding 9, 88
reverse engineering 358
RSC model 278
RTM 9, 88
RUC 246
rule of mixtures 181
runner system 73
RVE 236

S

second-order autocatalytic reaction 54
second-order reaction 54
shape functions 223, 225
shear modulus 44
shear thinning 41
sheet charge 373
sheet molding compound 60
shot size 67
sizing 36, 110
slit method 125
SMC 60
– stress-strain behavior 63
software 253
spherulite 46
squeezing flow 268
S-RIM 88
STAMAX™ 154
stiffness matrix 220
storage modulus 44
strain tensor 178
stress interactions 205
stress–strain curve
– time dependent 402
stress–strain relations 178, 184
stress tensor 178
structural properties 401

structural reaction injection molding 88
structural viscosity 41
structure simulation 334
substantial derivative 271

T

temperature shift factor 272
tensile modulus 385
tensile test 314, 416, 435
thermal conductivity 387
thermoplastics
– amorphous 43
– fiber-reinforced 372
– semi-crystalline 45
thermoset
– fiber-reinforced 372
three-noded element 222
time-temperature-transformation diagram 53
transformation matrices 185
transverse modulus 181
Tsai-Hill failure criterion 203
Tsai-Wu model 200
TTT-diagram 54
twin-screw extruder 376

U

unidirectional continuous fiber-reinforced laminate 179
unsaturated polyester 49, 57
urethane 50

V

vacuum-assisted resin infusion 10, 85
vacuum-assisted resin transfer molding 89
vacuum bagging techniques 83
VARI 10, 85
– ramp effect 87
VA-RTM 89
VG Studio MAX 118
vinyl ester 50
viscoelasticity
– compression molding 271
viscoelastic material properties 391
viscosity 42, 387
volume fraction 180
Volume Graphics 125

W

warpage 351, 355, 365, 391
weave 213
weight fraction 180
weight reduction 17
White-Metzner model 272
World Wide Failure Exercise 205
woven fabrics 31

X

X-ray 321
X-ray computed-tomography 117

Y

Young's modulus 396

Z

zero-order reaction 54